

# Weyl semimetal engineering by symmetry control in NiTe<sub>2</sub>

Marcos G. O. Junior, Augusto L. Araújo,<sup>\*</sup> Emmanuel V. C. Lopes,<sup>†</sup> and Tome M. Schmidt<sup>‡</sup>  
*Instituto de Física, Universidade Federal de Uberlândia, Uberlândia, MG 38400-902, Brazil*

In this work, we investigate the emergence of Weyl points in an inversion symmetry-breaking 1T-NiTe<sub>2</sub> system. Through first-principles calculations based on the density functional theory combined with tight-binding methods, distinct number of Weyl crossings arise under an appropriate symmetry breaking. We identify three sets of Weyl points by breaking the inversion symmetry in NiTe<sub>2</sub>, resulting in a total of 28 Weyl crossings. The first set comes from the Dirac semimetal, whereas the other two additional sets depend on the weight of the symmetry breaking. The topological characteristics of the Weyl semimetals have been investigated by computing the evolution of Wannier charge centers, providing their chiralities. Additionally, the bulk-boundary correspondence has been shown by computing the Fermi arcs. Our results provide a way for manipulating and creating distinct sets of Weyl points with appropriate external control, which can be valuable for applications in Weyltronics.

## I. INTRODUCTION

The Weyl fermions were theoretically predicted by Hermann Weyl in 1929 [1] as one of the particular cases of the Dirac equation. These particles behave as massless relativistic fermions, which arise in pairs with opposite chiralities [2–4]. Although predicted in high-energy physics, the only experimental observation of Weyl fermions remains in solid state physics, where they arise in the materials context under either time-reversal or inversion symmetry breaking [4–6]. Usually, Weyl crossings come from symmetry-protected Dirac semimetals (DSMs), with crossing points that are fourfold degenerate. Symmetry breaking raises the fourfold degeneracy, resulting in a pair of Weyl crossings with a defined chirality [4, 7]. Due to the Nielsen-Ninomiya theorem, the sum of chiralities over the Brillouin zone (BZ) must vanish [8]. Although the origin of Weyl points (WPs) is more commonly reported in symmetry-breaking DSMs, WPs can also arise from gapped Dirac cone systems [9].

Similarly to other topological phases of matter, driven by the bulk-boundary correspondence, Weyl semimetals also exhibit topological surface states, which are denominated Fermi arcs. Unlike other topological classes, where the surface states connect the valence to conduction bands, the Fermi arcs perform a non-closed curve in momentum space, connecting the bulk WPs with opposite chiralities projected onto the surface [3, 4]. Noncentrosymmetric XY compounds (X=Ta, Nb and Y=As, P) represent the first class of Weyl semimetal materials with Fermi arc properties that were theoretically predicted and experimentally observed [10–15]. Later, Weyl crossings have also been experimentally reported in additional noncentrosymmetric systems, such as MoTe<sub>2</sub> [16–19] and WTe<sub>2</sub> [20, 21], as well as in magnetic materials [22–25]. Weyl semimetals hold interesting properties, such as protected surface states [2, 4], negative magnetoresistance [26], and chiral anomaly [27, 28]. Those properties not only make this class of topological materials promising for applications in different subfields of condensed matter physics, including catalysis, thermoelectricity, quan-

tum computing, and superconductivity [29–34], but it is also a platform to realize and understand the concept of fundamental particles.

A particular class of materials promising for the study of Dirac semimetals is the transition metal dichalcogenides (TMDs). The TMD system has the form MX<sub>2</sub>, where M represents a transition metal, which is encapsulated by chalcogen atoms, denoted by X. These systems can crystallize in the 1T, 1T', and 2H structures, and the deposited layers are held together by van der Waals (vdW) interactions. Many examples of TMDs have been reported to present DSM phase and in some cases also Weyl properties, such as MTe<sub>2</sub> (M = Mo, W, Pd and Pt) [16, 20, 21, 35, 36] and PtSe<sub>2</sub> [37, 38]. Another interesting TMD is the centrosymmetric 1T-NiTe<sub>2</sub>, which has been widely studied and, through *ab initio* calculations and angle-resolved photoemission spectroscopy (ARPES) measurements, it has been verified to belong to the Dirac semimetal phase [39–41].

In this work, using first-principles and topological invariant calculations, we investigate the formation of multiple Weyl points in NiTe<sub>2</sub> under inversion symmetry breaking. We find that, by breaking the mirror  $\sigma_{xy}$  symmetry, the fourfold degenerate Dirac crossing splits into a pair of Weyl points with opposite chiralities near the Fermi level. Interestingly, beyond the two pairs of WPs originated from the Dirac semimetal phase, we find two additional sets of WPs coming out from gapped regions. The emergence of these additional sets depends not just on the symmetry, but also on the weight of the symmetry-breaking, resulting in additional 6 or 12 new pairs of WPs throughout the BZ. The topological nature of these additional WPs was verified by nonvanishing Berry curvature, Weyl chirality calculations, as well as their corresponding Fermi arcs. Our results provide a way to create sets of Weyl points in NiTe<sub>2</sub> by symmetry control.

## METHODOLOGY

First-principles calculations were performed using the density functional theory (DFT) [42, 43] within the gen-

eralized gradient approximation (GGA) for the exchange and correlation functional, employing the Perdew-Burke-Ernzerhof (PBE) parametrization [44]. A fully relativistic pseudopotential, within the projector augmented wave method (PAW) [45, 46], was used in the non-collinear spin-DFT formalism self-consistently. We have used the DFT codes Vienna *ab initio* Simulation Package (VASP) [47, 48] and Quantum Espresso (QE) [49, 50], with plane wave basis set with a cut-off energy of 400 eV. The Brillouin zone was sampled with a  $25 \times 25 \times 25$   $k$ -mesh grid (Monkhorst-Pack scheme) such that the total energy converges within the meV scale, and atomic structures are optimized requiring that the force on each atom to be less than 0.01 eV/Å. The analysis of the DFT results, including band structure plots, projections of orbital-atomic contributions, and isosurfaces plots, has been performed using the VASProcar post-processing code [51]. We build a tight-binding model based on DFT results by means of the Wannier90 package [52]. The topological properties, such as Chern number, Berry curvature, and Fermi arcs were investigated with Wannier-tools [53].

## II. RESULTS AND DISCUSSION

### Weyl crossings from Dirac Semimetal

1T-NiTe<sub>2</sub> is a semimetallic TMD, with strong intralayer bonds and vdW interactions between the layers. This system shows a hexagonal crystal structure, as illustrated in Fig. 1(a), with our fully optimized lattice parameters  $a = b = 3.90$  Å and  $c = 5.24$  Å. It belongs to the  $D_{3d}^3$  (or  $P\bar{3}m1$ ) space group symmetry, with time-reversal and inversion symmetry preserved. In this way, due to the Kramers degeneracy, the band dispersion must be doubly degenerate, and any crossing point would be at least fourfold degenerate. If such a crossing has linear dispersion, it is a strong candidate to be a DSM [54]. In the NiTe<sub>2</sub> system, a fourfold degenerate Dirac crossing has been reported along the  $\Gamma$ -A path [37, 39, 41], as indicated in Fig. 1(b). The high symmetry points  $\Gamma$  and A show the full  $D_{3d}$  symmetry, while the line connecting the points has a lower symmetry,  $C_{3v}$ .

The band structure of NiTe<sub>2</sub>, shown in Fig. 2(a), presents a linear crossing point close to the Fermi energy (-0.02 eV) along the  $\Gamma$ -A direction, a typical type-II DSM. It is interesting to note that, without SOC [Fig. 2(b)], this band crossing is sixfold degenerate. The inclusion of SOC lifts the band degeneracy at the crossing point, resulting in a fourfold degeneracy, as can be seen in Fig. 2(c). The DSM phase is intrinsic as a consequence of the symmetry protection, since there is no phase transition. Due to the SOC interaction, a double group symmetry analysis shows not only changes in the atomic orbital character, but also an inversion of the  $\Gamma_{4+}$  and  $\Gamma_{4-}$  bands at the high-symmetry A point. This inversion leads to the Dirac semimetal topological phase. The two-

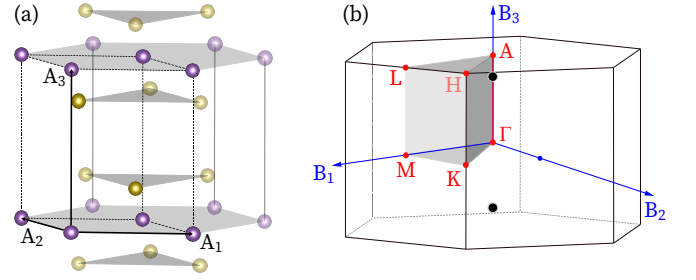


FIG. 1. (a) 1T-NiTe<sub>2</sub> crystal structure, identifying the unit cell with dashed lines. The purple and golden spheres represent the Ni and Te ions, respectively. The first Brillouin zone is shown in (b), where the black dots denote the DSM locations.

dimensional irreducible representations (IRREPs) of the states at the Dirac crossing  $\Gamma_{n-}$  and  $\Sigma_{m-}$  ( $m, n$  integers) are characterized by an opposite sign under  $C_3$  rotation [55]. In this way, the  $C_3$  symmetry avoids interaction between these states, preventing band gap opening and consequently imposing a Dirac crossing. As the system is a semimetal, we also confirmed the DSM topological phase by topological quantum chemistry analysis, in which the real space symmetry of the bands is included besides the topological properties in momentum space [56–58].

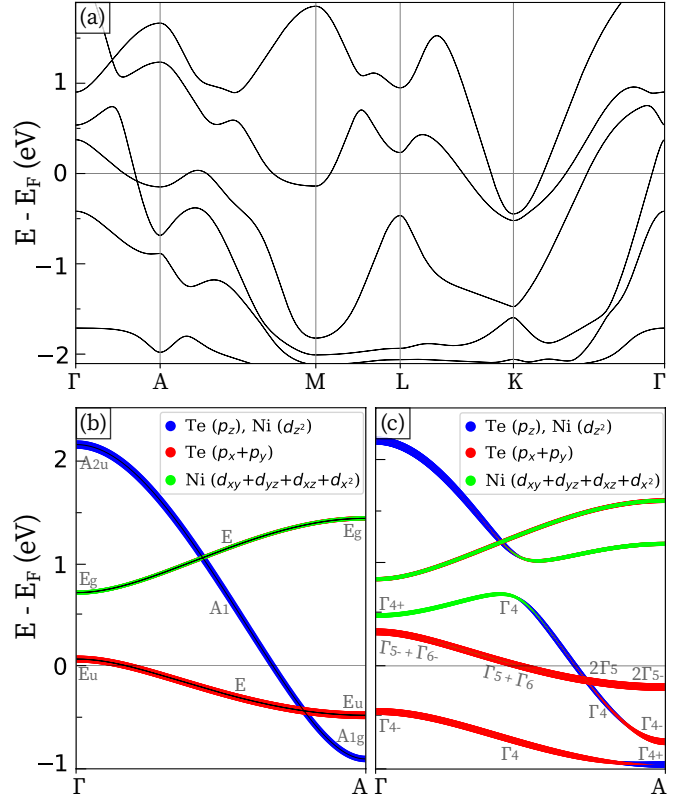


FIG. 2. 1T-NiTe<sub>2</sub> electronic band structure (a). Orbital projection from bands around the Fermi level along the  $\Gamma$ -A direction without (b) and with SOC (c). The bands are labeled with their corresponding IRREPs.

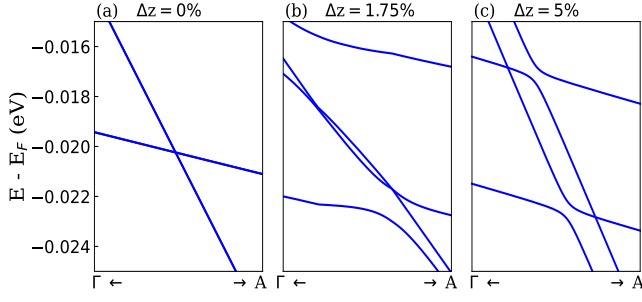


FIG. 3. Dirac semimetal in NiTe<sub>2</sub> (a) and its splitting into Weyl points under distinct inversion symmetry breaking weight (b) and (c).

The degeneracy of the DSM can be lifted upon breaking either inversion or time-reversal symmetry, allowing the emergence of Weyl semimetals. However, 1T-NiTe<sub>2</sub> is a centrosymmetric crystal, unlike other TMDs that are intrinsically noncentrosymmetric, such as 1T'-MoTe<sub>2</sub> and T<sub>d</sub>-WTe<sub>2</sub> [17–21]. To achieve a Weyl semimetal phase, we break the inversion symmetry, keeping the C<sub>3</sub> rotation, since it protects gapping, as previously discussed. In a practical way, this can be done by applying an electric field along the  $z$  direction of the structure in Fig. 1(a), or by the effect of a substrate, which also breaks the mirror  $\sigma_{xy}$  symmetry. In this work, we displace the Ni atom plane along the  $z$  direction, breaking the mirror  $\sigma_{xy}$  and consequently the inversion symmetry. This is equivalent to applying an electric field along the  $z$  direction, due to the distinct electronegativities of Ni and Te atoms. The symmetry of the point group will be reduced from D<sub>3d</sub> to C<sub>3v</sub>. As shown in Fig. 3, the fourfold DSM breaks into a pair of Weyl points aligned along the  $k_z$  direction. It preserves the type-II character, the same of the DSM. The displacement  $\Delta z$  in this figure is the relative percentage of the  $c$  lattice parameter. From Fig. 3, we note that the Weyl pairs distance increases by increasing the symmetry-breaking weight. The energy splitting between the Weyl pairs is only a few meV, and their chirality WPs distance is less than 0.005% of the reciprocal lattice parameter, making them hard to be detected. The respective Weyl points are located at (0.00000631, -0.00002383, 0.36463530) and (-0.00000971, 0.00001055, 0.36456357) in units of  $(2\pi/a, 2\pi/a, 2\pi/c)$ , for  $\Delta z = 5\%$ . The other two Weyl points from this set, henceforth denoted as set A, can be obtained by applying the time-reversal symmetry operation, which in a 3D system keeps the same chirality [59].

Weyl points from Dirac semimetals can also be obtained by breaking time-reversal symmetry. Recently, it has been shown that Cr-doped NiTe<sub>2</sub> induces ferromagnetic order, which leads to spin splitting in the Dirac semimetal, originating Weyl points near the Fermi energy [60].

### Emergence of additional sets of Weyl crossings

By breaking the inversion symmetry, we also verify the emergence of two additional sets of Weyl nodes. These crossing points arise from gapped regions under different weight of symmetry breaking, as illustrated in Fig. 4(a). We denote the additional sets of Weyl points as sets B and C. In the set B, represented by blue and red symbols, the topological phase transition from a trivial gapped region to a Weyl semimetal occurs at  $\Delta z = 1.75\%$  [Fig. 4(b)]. It can be seen pairs of linear touching points occurring at symmetric positions, typically a type-I Weyl semimetal.

By increasing the crystal field distortion, the set C emerges at  $\Delta z = 3\%$ , as can be seen in Fig. 4(c). In this picture, we observe a tilted crossing behavior that is a key signature of type-II Weyl crossings. It is worth noting that both additional sets of WPs (sets B and C) emerge from the same bands of the set A, the one coming from the Dirac semimetal. For the highest distortion investigated in this work ( $\Delta z = 5\%$ ), the crossing points of sets B and C are localized below the Fermi level at -0.89 eV and -1.41 eV, respectively.

The weight for the displacement  $\Delta z$  affects the WP energy as well as its position in the BZ. For the highest distortion [Fig 4(a)], we have four WPs in the first BZ (denoted by the green marked region), two of them come from the set B and two from set C. The coordinates of the set B, in units of  $(2\pi/a, 2\pi/a, 2\pi/c)$ , are (0.2348, -0.1844, 0.3283) and (0.2332, -0.04809, -0.3321), indicated by the blue square and red circle, respectively. For set C, in the same units, the respective coordinates are (0.3245, -0.0305, -0.2212) and (0.3239, -0.2928, 0.2217), indicated by the purple circle and yellow square. The other WP coordinates can be obtained from these four WPs by applying the following symmetries: C<sub>3</sub>, time-reversal and vertical mirror. While C<sub>3</sub> and time-reversal leads to a WP with the same chirality, the vertical mirror reverse the chirality of each WP.

The WPs have also been investigated by scanning any crossing bands in the first BZ. This analysis ensures that we count all Weyl nodes. The Weyl point positions can be determined by computing the energy isosurface  $|\Delta E| = |E_c - E_v|$  between the bands around the Fermi level, within the entire BZ. Here  $E_c$  and  $E_v$  denote the two bands that originate the Dirac semimetal, as shown in Fig. 2. For a touching point, this difference will go to zero. In Fig. 4(d) we show a projection of  $|\Delta E|$  around a square volume containing a pair of WPs from each distinct set. As can be seen in the zoomed picture,  $|\Delta E|$  goes to zero at the crossing point.

To investigate the topological properties of each Weyl crossing candidate, we calculate the Weyl chirality ( $\chi$ ). For each crossing point, our results show  $\chi = \pm 1$ . The chiralities are shown in Figure 4(a), illustrated by the colors red (set B) and yellow (set C) for the positive chiral charge, while the blue (set B) and purple (set C) represent the negative Weyl chiralities. The sum of all

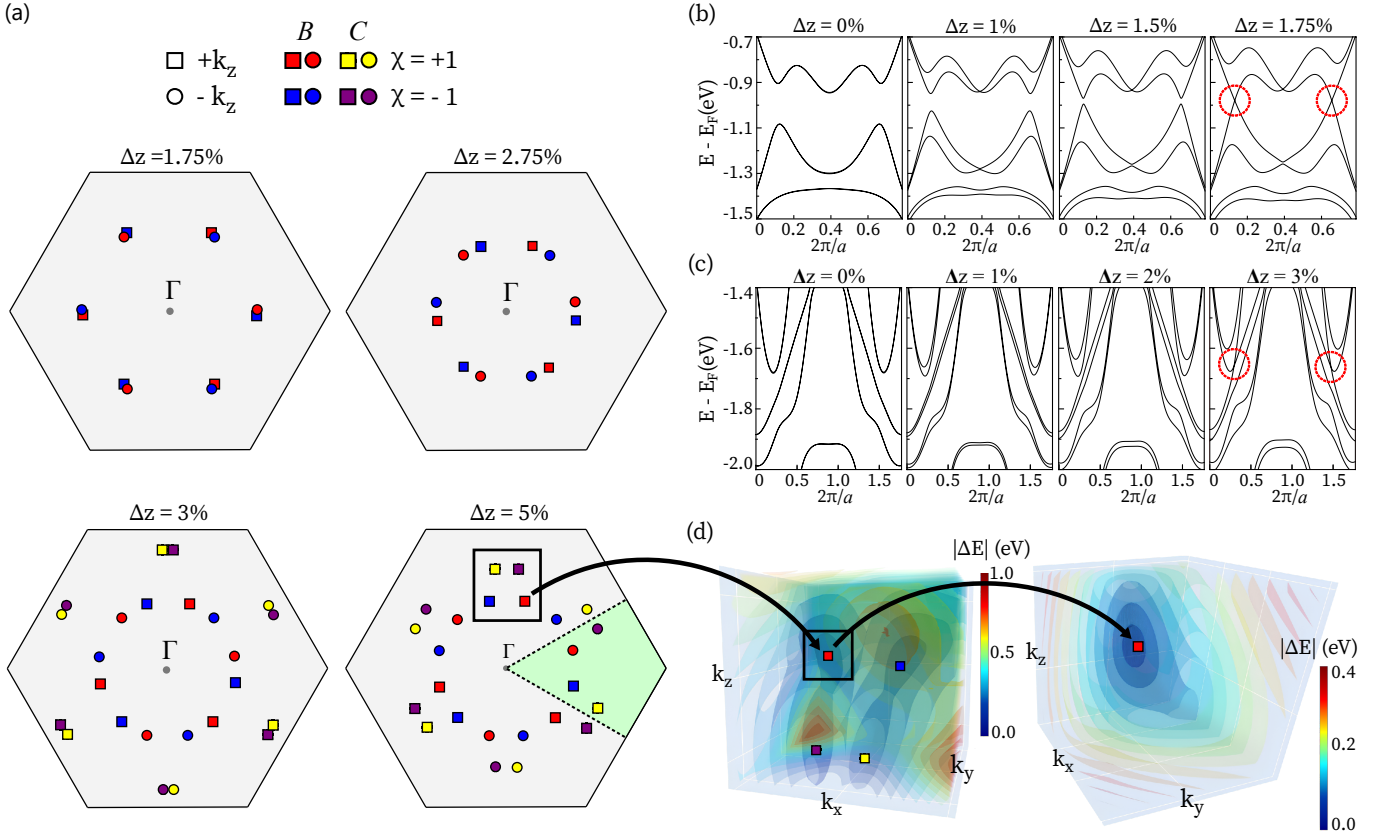


FIG. 4. (a) Evolution of Weyl point locations as a function of the symmetry breaking weight ( $\Delta z$ ) for sets  $B$  (blue and red) and  $C$  (yellow and purple). The band structures in (b) and (c) show the emergence of Weyl crossings of sets  $B$  and  $C$ , respectively. The corresponding isoenergy surface plot, illustrating the Weyl point positions (d).

chiral charges in the entire Brillouin zone vanishes, in agreement with the Nielsen-Ninomiya theorem [8]. One of the key properties of the Weyl semimetals is the Berry curvature, which is given by  $\Omega = \pm \mathbf{k}/2k^3$  in a 3D system. This allows to visualize the Weyl points with positive or negative Weyl chirality as a source or drain of Berry curvature, respectively. To illustrate this, we show in Fig. 5(a) the Berry curvature plot for a given plane of constant  $k_z$ . We also compute the evolution of Wannier charge centers (WCCs) for the selected crossing points, which further confirms the nontrivial behavior [Figs. 5(c) and 5(e)].

### Fermi arcs

To further confirm the topological properties of NiTe<sub>2</sub>, we investigate its bulk-boundary correspondence by building a sufficiently large slab. Using a slab of 35 stacked unit layers and a distortion of  $\Delta z = 5\%$ , we search for the Fermi arcs. The topological surface states were investigated on the (001) surface in both ways, energy- and momentum-resolved density of states. Figures 6(a) and 6(c) show the momentum-resolved electronic density of states for a fixed energy cut at  $-0.89$  eV

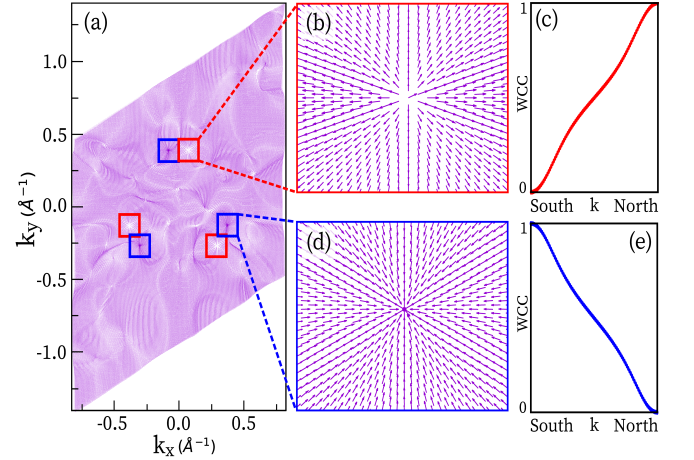


FIG. 5. Berry curvature plot for a constant  $k_z$  plane in the first Brillouin zone (a). Zoom of two Weyl points illustrating the source (b) and drain (d) of Berry curvature, and their corresponding evolution of WCCs in (c) and (e), respectively.

and  $-1.41$  eV below the Fermi level, respectively. These values represent the energy cut at which the WPs from sets  $B$  and  $C$  emerge. The red and yellow (blue and purple) symbols in Figs. 6(a) and 6(c) represent the WPs

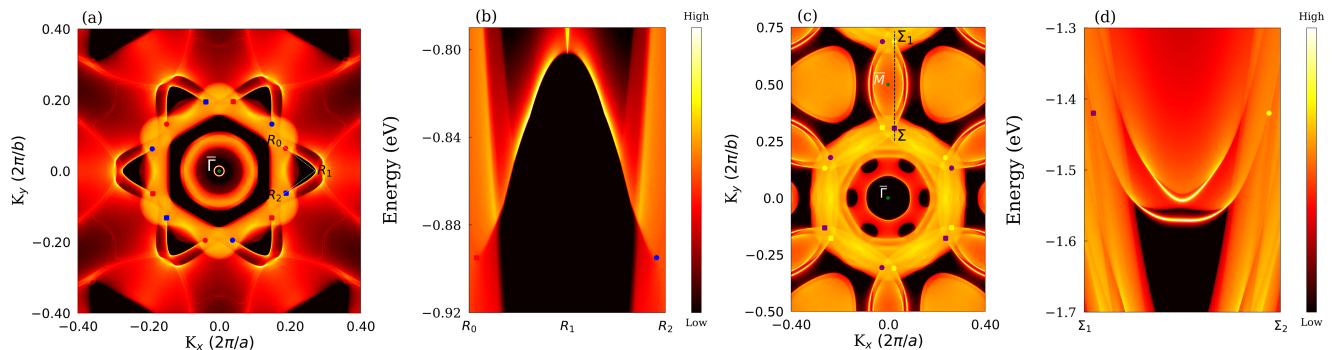


FIG. 6. (a) Momentum-resolved electronic density of states for the energy cut at -0.89 eV on the (001) surface, for set  $B$  of Weyl points. (b) Energy-resolved dispersion along the  $R_0$ - $R_1$ - $R_2$ , indicated by the white line in (a). In (c) and (d) are the momentum- and energy-resolved plots for the set  $C$  of Weyl points, with a fixed cut at -1.41 eV.

with positive (negative) chirality of sets  $B$  and  $C$ , respectively. In both systems, one surface state emerges at the bulk-projected WP, forming a non-closed curve that connects to its respective opposite chiral pair.

The energy-resolved plots [Figs. 6(b) and 6(d)] show the band dispersion along the  $R_0$ - $R_1$ - $R_2$  and  $\Sigma$ - $\Sigma_1$  paths, as indicated in Figs. 6(a) and 6(c), respectively. For set  $B$  of WPs, one high intensity surface state can be seen at the interface with the bulk states. By means of energy-resolved density of states, this state can be seen emerging at the bulk WP projection on the surface, and showing a parabolic dispersion until it reaches its respective pair. For the set  $C$  of Weyl crossings, the high intensity topological surface state shows an energy dispersion around 0.15 eV, achieving the minimal point in -1.57 eV, as shown in Fig. 6(d).

### III. CONCLUSIONS

In summary, based on first-principles and topological invariant calculations, we show a process for exploring Weyl semimetals by controlling the symmetry breaking in 1T-NiTe<sub>2</sub>. We show that the predicted Dirac semimetal in NiTe<sub>2</sub> splits into a pair of type-II Weyl points by breaking the inversion symmetry, since the time-reversal symmetry is preserved. The inversion symmetry control has been performed by breaking the planar mirror  $\sigma_{xy}$  sym-

metry, which could be experimentally performed by applying an electric field along the  $z$  direction, or just by the effect of an appropriate substrate. Our results reveal additional sets of Weyl points, beyond those originating from the Dirac semimetal, coming out of gapped regions of the first Brillouin zone. The emergence of those unexpected sets of Weyl crossings is dependent on the weight of the symmetry breaking. For any symmetry breaking, the first set coming from the Dirac semimetal is always present near the Fermi level. Under a certain breaking weight, an additional set of Weyls emerges around -0.89 eV, and for a further strength, another set of Weyls is revealed around -1.41 eV from the Fermi level. Both additional sets present 6 pairs of Weyl nodes, the former being type-I while the second is type-II. This procedure for manipulating and creating Weyl semimetals, resulting in on/off of topological surface states, can be suitable for applications in Weyltronics.

### ACKNOWLEDGMENTS

The authors acknowledge CAPES (Financial Code 001), CNPq, FAPEMIG and INCT-Nanocarbono for the financial support. The authors also acknowledge LNCC (project SCAFMAT2) and CENAPAD-SP (project proj483) for the computational time.

\* [augusto.araujo@ilum.cnpem.br](mailto:augusto.araujo@ilum.cnpem.br); Present address: Ilum School of Science, Brazilian Center for Research in Energy and Materials (CNPem), 13083-970, Campinas, SP, Brazil

† [emmanuel.lopes@ufu.br](mailto:emmanuel.lopes@ufu.br)

‡ [tschmidt@ufu.br](mailto:tschmidt@ufu.br)

<sup>1</sup> Hermann Weyl *et al.*, “Electron and gravitation,” *z. Phys* **56**, 330–352 (1929).

<sup>2</sup> N. P. Armitage, E. J. Mele, and Ashvin Vishwanath, “Weyl and dirac semimetals in three-dimensional solids,”

*Rev. Mod. Phys.* **90**, 015001 (2018).

<sup>3</sup> Binghai Yan and Claudia Felser, “Topological materials: Weyl semimetals,” *Annual Review of Condensed Matter Physics* **8**, 337–354 (2017).

<sup>4</sup> M. Zahid Hasan, Su-Yang Xu, Ilya Belopolski, and Shin-Ming Huang, “Discovery of weyl fermion semimetals and topological fermi arc states,” *Annual Review of Condensed Matter Physics* **8**, 289–309 (2017).

<sup>5</sup> Shengyuan A. Yang, “Dirac and weyl materials: Fundamental aspects and some spintronics applications,” *SPIN*

- 06**, 1640003 (2016).
- <sup>6</sup> Mengyao Qi, Chao An, Yonghui Zhou, Hao Wu, Bowen Zhang, Chunhua Chen, Yifang Yuan, Shuyang Wang, Ying Zhou, Xuliang Chen, *et al.*, “Pressure-driven lifshitz transition in type-ii dirac semimetal nite 2,” *Physical Review B* **101**, 115124 (2020).
  - <sup>7</sup> A.A. Burkov, “Weyl metals,” *Annual Review of Condensed Matter Physics* **9**, 359–378 (2018).
  - <sup>8</sup> H.B. Nielsen and Masao Ninomiya, “The adler-bell-jackiw anomaly and weyl fermions in a crystal,” *Physics Letters B* **130**, 389–396 (1983).
  - <sup>9</sup> Qiangsheng Lu, P. V. Sreenivasa Reddy, Hyeon Jeon, Alessandro R. Mazza, Matthew Brahlek, Weikang Wu, Shengyuan A. Yang, Jacob Cook, Clayton Conner, Xiaojian Zhang, Amarnath Chakraborty, Yueh-Ting Yao, Hung-Ju Tien, Chun-Han Tseng, Po-Yuan Yang, Shang-Wei Lien, Hsin Lin, Tai-Chang Chiang, Giovanni Vignale, An-Ping Li, Tay-Rong Chang, Rob G. Moore, and Guang Bian, “Realization of a two-dimensional weyl semimetal and topological fermi strings,” *Nature Communications* **15** (2024), 10.1038/s41467-024-50329-6.
  - <sup>10</sup> Su-Yang Xu, Ilya Belopolski, Nasser Alidoust, Madhab Neupane, Guang Bian, Chenglong Zhang, Raman Sankar, Guoqing Chang, Zhujun Yuan, Chi-Cheng Lee, Shin-Ming Huang, Hao Zheng, Jie Ma, Daniel S. Sanchez, BaoKai Wang, Arun Bansil, Fangcheng Chou, Pavel P. Shibayev, Hsin Lin, Shuang Jia, and M. Zahid Hasan, “Discovery of a weyl fermion semimetal and topological fermi arcs,” *Science* **349**, 613–617 (2015).
  - <sup>11</sup> Su-Yang Xu, Nasser Alidoust, Ilya Belopolski, Zhujun Yuan, Guang Bian, Tay-Rong Chang, Hao Zheng, Vladimir N. Strocov, Daniel S. Sanchez, Guoqing Chang, Chenglong Zhang, Daixiang Mou, Yun Wu, Lunan Huang, Chi-Cheng Lee, Shin-Ming Huang, BaoKai Wang, Arun Bansil, Horng-Tay Jeng, Titus Neupert, Adam Kaminski, Hsin Lin, Shuang Jia, and M. Zahid Hasan, “Discovery of a weyl fermion state with fermi arcs in niobium arsenide,” *Nature Physics* **11**, 748–754 (2015).
  - <sup>12</sup> Su-Yang Xu, Ilya Belopolski, Daniel S. Sanchez, Chenglong Zhang, Guoqing Chang, Cheng Guo, Guang Bian, Zhujun Yuan, Hong Lu, Tay-Rong Chang, Pavel P. Shibayev, Mykhailo L. Prokopych, Nasser Alidoust, Hao Zheng, Chi-Cheng Lee, Shin-Ming Huang, Raman Sankar, Fangcheng Chou, Chuang-Han Hsu, Horng-Tay Jeng, Arun Bansil, Titus Neupert, Vladimir N. Strocov, Hsin Lin, Shuang Jia, and M. Zahid Hasan, “Experimental discovery of a topological weyl semimetal state in tap,” *Science Advances* **1**, e1501092 (2015).
  - <sup>13</sup> L. X. Yang, Z. K. Liu, Y. Sun, H. Peng, H. F. Yang, T. Zhang, B. Zhou, Y. Zhang, Y. F. Guo, M. Rahn, D. Prabhakaran, Z. Hussain, S.-k. Mo, C. Felser, B. Yan, and Y. L. Chen, “Weyl semimetal phase in the non-centrosymmetric compound TaAs,” *Nature Physics* **11**, 728–732 (2015).
  - <sup>14</sup> B. Q. Lv, H. M. Weng, B. B. Fu, X. P. Wang, H. Miao, J. Ma, P. Richard, X. C. Huang, L. X. Zhao, G. F. Chen, Z. Fang, X. Dai, T. Qian, and H. Ding, “Experimental discovery of weyl semimetal taas,” *Phys. Rev. X* **5**, 031013 (2015).
  - <sup>15</sup> Z. K. Liu, L. X. Yang, Y. Sun, T. Zhang, H. Peng, H. F. Yang, C. Chen, Y. Zhang, Y. F. Guo, D. Prabhakaran, M. Schmidt, Z. Hussain, S.-K. Mo, C. Felser, B. Yan, and Y. L. Chen, “Evolution of the fermi surface of weyl semimetals in the transition metal pnictide family,” *Nature Materials* **15**, 27–31 (2015).
  - <sup>16</sup> Yan Sun, Shu-Chun Wu, Mazhar N. Ali, Claudia Felser, and Binghai Yan, “Prediction of weyl semimetal in orthorhombic mote<sub>2</sub>,” *Phys. Rev. B* **92**, 161107 (2015).
  - <sup>17</sup> J. Jiang, Z.K. Liu, Y. Sun, H.F. Yang, C.R. Rajamathi, Y.P. Qi, L.X. Yang, C. Chen, H. Peng, C.-C. Hwang, S.Z. Sun, S.-K. Mo, I. Vobornik, J. Fujii, S.S.P. Parkin, C. Felser, B.H. Yan, and Y.L. Chen, “Signature of type-ii weyl semimetal phase in mote<sub>2</sub>,” *Nature Communications* **8** (2017), 10.1038/ncomms13973.
  - <sup>18</sup> Zhijun Wang, Dominik Gresch, Alexey A. Soluyanov, Weiwei Xie, S. Kushwaha, Xi Dai, Matthias Troyer, Robert J. Cava, and B. Andrei Bernevig, “mote<sub>2</sub>: A type-ii weyl topological metal,” *Phys. Rev. Lett.* **117**, 056805 (2016).
  - <sup>19</sup> Anna Tamai, QS Wu, Irène Cucchi, Flavio Yair Bruno, Sara Riccò, Timur K Kim, Moritz Hoesch, Céline Barreteau, Enrico Giannini, Céline Besnard, *et al.*, “Fermi arcs and their topological character in the candidate type-ii weyl semimetal mote 2,” *Physical Review X* **6**, 031021 (2016).
  - <sup>20</sup> Yun Wu, Daixiang Mou, Na Hyun Jo, Kewei Sun, Lunan Huang, S. L. Bud’ko, P. C. Canfield, and Adam Kaminski, “Observation of fermi arcs in the type-ii weyl semimetal candidate wte<sub>2</sub>,” *Phys. Rev. B* **94**, 121113 (2016).
  - <sup>21</sup> Chenlu Wang, Yan Zhang, Jianwei Huang, Simin Nie, Guodong Liu, Aiji Liang, Yuxiao Zhang, Bing Shen, Jing Liu, Cheng Hu, Ying Ding, Defa Liu, Yong Hu, Shaolong He, Lin Zhao, Li Yu, Jin Hu, Jiang Wei, Zhiqiang Mao, Youguo Shi, Xiaowen Jia, Fengfeng Zhang, Shenjin Zhang, Feng Yang, Zhimin Wang, Qinqun Peng, Hongming Weng, Xi Dai, Zhong Fang, Zuyan Xu, Chuangtian Chen, and X. J. Zhou, “Observation of fermi arc and its connection with bulk states in the candidate type-ii weyl semimetal wte<sub>2</sub>,” *Phys. Rev. B* **94**, 241119 (2016).
  - <sup>22</sup> D. F. Liu, A. J. Liang, E. K. Liu, Q. N. Xu, Y. W. Li, C. Chen, D. Pei, W. J. Shi, S. K. Mo, P. Dudin, T. Kim, C. Cacho, G. Li, Y. Sun, L. X. Yang, Z. K. Liu, S. S. P. Parkin, C. Felser, and Y. L. Chen, “Magnetic weyl semimetal phase in a kagomé crystal,” *Science* **365**, 1282–1285 (2019).
  - <sup>23</sup> Noam Morali, Rajib Batabyal, Pranab Kumar Nag, Enke Liu, Qiunan Xu, Yan Sun, Binghai Yan, Claudia Felser, Nurit Avraham, and Haim Beidenkopf, “Fermi-arc diversity on surface terminations of the magnetic weyl semimetal co<sub>3</sub>sn<sub>2</sub>s<sub>2</sub>,” *Science* **365**, 1286–1291 (2019).
  - <sup>24</sup> Benjamin Schruck, Yevhen Kushnirenko, Brinda Kuthanazhi, Junyeong Ahn, Lin-Lin Wang, Evan O’Leary, Kyunghan Lee, Andrew Eaton, Alexander Fedorov, Rui Lou, Vladimir Voroshnin, Oliver J. Clark, Jaime Sánchez-Barriga, Sergey L. Bud’ko, Robert-Jan Slager, Paul C. Canfield, and Adam Kaminski, “Emergence of fermi arcs due to magnetic splitting in an antiferromagnet,” *Nature* **603**, 610–615 (2022).
  - <sup>25</sup> Niels B. M. Schröter, Iñigo Robredo, Sebastian Klemenz, Robert J. Kirby, Jonas A. Krieger, Ding Pei, Tianlun Yu, Samuel Stolz, Thorsten Schmitt, Pavel Dudin, Timur K. Kim, Cephise Cacho, Andreas Schnyder, Aitor Bergara, Vladimir N. Strocov, Fernando de Juan, Maia G. Vergniory, and Leslie M. Schoop, “Weyl fermions, fermi arcs, and minority-spin carriers in ferromagnetic cos<sub>2</sub>,” *Science Advances* **6** (2020), 10.1126/sciadv.abd5000.
  - <sup>26</sup> Xiaochun Huang, Lingxiao Zhao, Yujia Long, Peipei Wang, Dong Chen, Zhanhai Yang, Hui Liang, Mianqi Xue, Hongming Weng, Zhong Fang, Xi Dai, and Genfu Chen, “Ob-

- servation of the chiral-anomaly-induced negative magnetoresistance in 3d weyl semimetal taas,” *Physical Review X* **5** (2015), 10.1103/physrevx.5.031023.
- 27 N. P. Ong and Sihang Liang, “Experimental signatures of the chiral anomaly in dirac–weyl semimetals,” *Nature Reviews Physics* **3**, 394–404 (2021).
  - 28 Cheng-Long Zhang, Su-Yang Xu, Ilya Belopolski, Zhujun Yuan, Ziquan Lin, Bingbing Tong, Guang Bian, Nasser Alidoust, Chi-Cheng Lee, Shin-Ming Huang, Tay-Rong Chang, Guoqing Chang, Chuang-Han Hsu, Horng-Tay Jeng, Madhab Neupane, Daniel S. Sanchez, Hao Zheng, Junfeng Wang, Hsin Lin, Chi Zhang, Hai-Zhou Lu, Shun-Qing Shen, Titus Neupert, M. Zahid Hasan, and Shuang Jia, “Signatures of the adler–bell–jackiw chiral anomaly in a weyl fermion semimetal,” *Nature Communications* **7** (2016), 10.1038/ncomms10735.
  - 29 Tobias Meng and Leon Balents, “Weyl superconductors,” *Physical Review B* **86**, 054504 (2012).
  - 30 Grigory Bednik, AA Zyuzin, and AA Burkov, “Superconductivity in weyl metals,” *Physical Review B* **92**, 035153 (2015).
  - 31 Yi Li and F. D. M Haldane, “Topological nodal cooper pairing in doped weyl metals,” *Physical Review Letters* **120**, 067003 (2018).
  - 32 P. O. Sukhachov and E. V. Gorbar, “Superconductivity in weyl semimetals in a strong pseudomagnetic field,” *Phys. Rev. B* **102**, 014513 (2020).
  - 33 Fei Han, Nina Andrejevic, Thanh Nguyen, Vladyslav Kozii, Quynh T. Nguyen, Tom Hogan, Zhiwei Ding, Ricardo Pablo-Pedro, Shreya Parjan, Brian Skinner, Ahmet Alatas, Ercan Alp, Songxue Chi, Jaime Fernandez-Baca, Shengxi Huang, Liang Fu, and Mingda Li, “Quantized thermoelectric hall effect induces giant power factor in a topological semimetal,” *Nature Communications* **11** (2020), 10.1038/s41467-020-19850-2.
  - 34 Hanggara Sudrajat, “Topological quantum materials in catalysis,” *Journal of Materials Chemistry A* **13**, 6325–6341 (2025).
  - 35 H. Leng, C. Paulsen, Y. K. Huang, and A. de Visser, “Type-i superconductivity in the dirac semimetal  $\text{PtTe}_2$ ,” *Phys. Rev. B* **96**, 220506 (2017).
  - 36 Mingzhe Yan, Huaqing Huang, Kenan Zhang, Eryin Wang, Wei Yao, Ke Deng, Guoliang Wan, Hongyun Zhang, Masashi Arita, Haitao Yang, Zhe Sun, Hong Yao, Yang Wu, Shoushan Fan, Wenhui Duan, and Shuyun Zhou, “Lorentz-violating type-ii dirac fermions in transition metal dichalcogenide  $\text{PtTe}_2$ ,” *Nature Communications* **8** (2017), 10.1038/s41467-017-00280-6.
  - 37 Franz Fischer, Abderrezak Torche, Marta Prada, and Gabriel Bester, “ $g\omega$  effects on the topology of type-ii dirac cones in  $\text{nTe}_2$ ,  $\text{PtSe}_2$ , and  $\text{PtTe}_2$ ,” *Phys. Rev. B* **110**, 165146 (2024).
  - 38 Huaqing Huang, Shuyun Zhou, and Wenhui Duan, “Type-ii dirac fermions in the  $\text{PtSe}_2$  class of transition metal dichalcogenides,” *Phys. Rev. B* **94**, 121117 (2016).
  - 39 Jie Zhang and G Q Huang, “The superconductivity and topological surface state of type-ii dirac semimetal  $\text{nTe}_2$ ,” *Journal of Physics: Condensed Matter* **32**, 205702 (2020).
  - 40 Libo Zhang, Zhiqingzi Chen, Kaixuan Zhang, Lin Wang, Huang Xu, Li Han, Wanlong Guo, Yao Yang, Chianung Kuo, Chin Shan Lue, Debashis Mondal, Jun Fuji, Ivana Vobornik, Barun Ghosh, Amit Agarwal, Huaizhong Xing, Xiaoshuang Chen, Antonio Politano, and Wei Lu, “High-frequency rectifiers based on type-ii dirac fermions,” *Nature Communications* **12** (2021), 10.1038/s41467-021-21906-w.
  - 41 Joseph A. Hlevyack, Liang-Ying Feng, Meng-Kai Lin, Rovi Angelo B. Villaos, Ro-Ya Liu, Peng Chen, Yao Li, Sung-Kwan Mo, Feng-Chuan Chuang, and T.-C. Chiang, “Dimensional crossover and band topology evolution in ultrathin semimetallic  $\text{nTe}_2$  films,” *npj 2D Materials and Applications* **5** (2021), 10.1038/s41699-021-00218-z.
  - 42 P. Hohenberg and W. Kohn, “Inhomogeneous electron gas,” *Phys. Rev.* **136**, B864–B871 (1964).
  - 43 W. Kohn and L. J. Sham, “Self-consistent equations including exchange and correlation effects,” *Phys. Rev.* **140**, A1133–A1138 (1965).
  - 44 J. P. Perdew, K. Burke, and M. Ernzerhof, “Generalized gradient approximation made simple,” *Phys. Rev. Lett.* **77**, 3865 (1996).
  - 45 P. E. Blöchl, “Projector augmented-wave method,” *Phys. Rev. B* **50**, 17953–17979 (1994).
  - 46 Andrea Dal Corso, “Projector augmented-wave method: Application to relativistic spin-density functional theory,” *Phys Rev B* **82**, 075116 (2010).
  - 47 G. Kresse and J. Furthmüller, “Efficiency of ab-initio total energy calculations for metals and semiconductors using a plane-wave basis set,” *Computational Materials Science* **6**, 15 – 50 (1996).
  - 48 G. Kresse and J. Furthmüller, “Efficient iterative schemes for ab initio total-energy calculations using a plane-wave basis set,” *Phys. Rev. B* **54**, 11169–11186 (1996).
  - 49 Paolo Giannozzi, Stefano Baroni, Nicola Bonini, Matteo Calandra, Roberto Car, Carlo Cavazzoni, Davide Ceresoli, Guido L Chiarotti, Matteo Cococcioni, Ismaila Dabo, Andrea Dal Corso, Stefano de Gironcoli, Stefano Fabris, Guido Fratesi, Ralph Gebauer, Uwe Gerstmann, Christos Gougousis, Anton Kokalj, Michele Lazzeri, Layla Martin-Samos, Nicola Marzari, Francesco Mauri, Riccardo Mazzarello, Stefano Paolini, Alfredo Pasquarello, Lorenzo Paulatto, Carlo Sbraccia, Sandro Scandolo, Gabriele Sclauzero, Ari P Seitsonen, Alexander Smogunov, Paolo Umari, and Renata M Wentzcovitch, “QUANTUM ESPRESSO: a modular and open-source software project for quantum simulations of materials,” *J. Phys.: Condens. Matter* **21**, 395502 (2009).
  - 50 P Giannozzi, O Andreussi, T Brumme, O Bunau, M Buongiorno Nardelli, M Calandra, R Car, C Cavazzoni, D Ceresoli, M Cococcioni, N Colonna, I Carnimeo, A Dal Corso, S de Gironcoli, P Delugas, R A DiStasio, A Ferretti, A Floris, G Fratesi, G Fugallo, R Gebauer, U Gerstmann, F Giustino, T Gorni, J Jia, M Kawamura, H-Y Ko, A Kokalj, E Küçükbenli, M Lazzeri, M Marsili, N Marzari, F Mauri, N L Nguyen, H-V Nguyen, A Otero de-la Roza, L Paulatto, S Poncé, D Rocca, R Sabatini, B Santra, M Schlipf, A P Seitsonen, A Smogunov, I Timrov, T Thonhauser, P Umari, N Vast, X Wu, and S Baroni, “Advanced capabilities for materials modelling with quantum ESPRESSO,” *J. Phys.: Condens. Matter* **29**, 465901 (2017).
  - 51 A. L. Araújo and R. P. Maciel, “Vasprocar: Python tools for dft calculations,” (2023).
  - 52 Giovanni Pizzi, Valerio Vitale, Ryotaro Arita, Stefan Blügel, Frank Freimuth, Guillaume Géranton, Marco Gibertini, Dominik Gresch, Charles Johnson, Takashi Koretsune, *et al.*, “Wannier90 as a community code: new features and applications,” *Journal of Physics: Condensed Matter* **32**, 165902 (2020).

- <sup>53</sup> QuanSheng Wu, ShengNan Zhang, Hai-Feng Song, Matthias Troyer, and Alexey A Soluyanov, “Wanniertools: An open-source software package for novel topological materials,” *Computer Physics Communications* **224**, 405–416 (2018).
- <sup>54</sup> Jiaheng Li, Zetao Zhang, Chong Wang, Huaqing Huang, Bing-Lin Gu, and Wenhui Duan, “Topological semimetals from the perspective of first-principles calculations,” *Journal of Applied Physics* **128** (2020), 10.1063/5.0025396.
- <sup>55</sup> George F Koster, “Space groups and their representations,” in *Solid state physics*, Vol. 5 (Elsevier, 1957) pp. 173–256.
- <sup>56</sup> Jorrit Kruthoff, Jan de Boer, Jasper van Wezel, Charles L. Kane, and Robert-Jan Slager, “Topological Classification of Crystalline Insulators through Band Structure Combinatorics,” *Phys. Rev. X* **7**, 041069 (2017).
- <sup>57</sup> Barry Bradlyn, Luis Elcoro, Jennifer Cano, Maia G Vergniory, Zhijun Wang, Claudia Felser, Mois I Aroyo, and B Andrei Bernevig, “Topological quantum chemistry,” *Nature* **547**, 298–305 (2017).
- <sup>58</sup> MG Vergniory, L Elcoro, Claudia Felser, Nicolas Regnault, B Andrei Bernevig, and Zhijun Wang, “A complete catalogue of high-quality topological materials,” *Nature* **566**, 480–485 (2019).
- <sup>59</sup> David Vanderbilt, *Berry Phases in Electronic Structure Theory: Electric Polarization, Orbital Magnetization and Topological Insulators* (Cambridge University Press, 2018).
- <sup>60</sup> Liguozhang, Dapeng Zhao, Xiangyang Liu, Junwen Lai, Junhai Ren, Qin Wang, Haicheng Lin, Yan Sun, and Katsumi Tanigaki, “Molecular beam epitaxy growth and doping modulation of topological semimetal nite2,” *Applied Physics Letters* **125** (2024), 10.1063/5.0220320.